Theor Chem Acc (2004) 111:132–140
DOI 10.1007/s00214-003-0517-4

Theoretical
Chemistry Accounts

Regular article

Solvent effects on *g*-tensors of semiquinone radical anions: polarizable continuum versus cluster models

I. Ciofini[1], **R. Reviakine**[2], **A. Arbuznikov**[2], **M. Kaupp**[2]

[1] Laboratoire d'Electrochimie et Chimie Analytique, UMR7575, Ecole Nationale Supérieure de Chimie de Paris, 11, rue Pierre et Marie Curie, Paris, France
[2] Institut für Anorganische Chemie, Universität Würzburg, Am Hubland, Würzburg, Germany

Received: 18 February 2003 / Revised: 30 April 2003 / Published online: 6 February 2004

Abstract. Density functional theory has been applied to study environmental effects on electronic *g*-tensors of a series of 1,4 semiquinone radical anions. In particular, solvent effects on solute structure, spin density distribution, and *g*-tensor have been investigated using both the conductor-like polarizable continuum model (CPCM) and explicit cluster solvent models. For protic solvents, the CPCM calculations provide solvent effects in qualitative but not in quantitative agreement with experiment. Explicit inclusion of solvent molecules hydrogen-bonded to the semiquinone oxygen atoms is required to obtain a more quantitative description. Available experimental *g*-tensor data in aprotic solvents are insufficient to judge adequately the performance of the CPCM calculations. However, the present data should serve to calibrate future experimental electron paramagnetic resonance studies. Detailed molecular-orbital analyses of the solvent influences on the *g*-tensors of various semiquinone radical anions are provided.

Keywords: Continuum solvent model – Density functional theory – Electronic *g*-tensor – Photosynthesis – Semiquinones

Introduction

With the development of high-field electron paramagnetic resonance (EPR) spectroscopy in the last decade, the accurate resolution of *g*-tensor anisotropy has become possible also for organic radicals [1, 2, 3, 4, 5, 6, 7, 8, 9, 10, 11, 12, 13, 14, 15, 16, 17, 18, 19]. This provides a new important experimental tool for the indirect inspection of the spin density distribution of, for instance, biologically relevant radicals. As the EPR parameters (*g*- and *A*-tensors) may be affected significantly by small changes in electron density distribution, they are important probes of the environment around the molecule.

The present study is focused on *g*-tensors of semiquinone radical anions. As these radicals are intermediates in many of the major biological redox processes (e.g. in photosynthesis and in respiration [20]), they have been the subject of many high-field EPR studies, both in protein environments and in isotropic solution [1, 2, 3, 4, 5, 6, 7, 8, 9, 10, 11, 12, 13, 14, 15, 16, 17, 18, 19, 21, 22, 23, 24, 25, 26]. In particular, the *g*-tensor of semiquinones (as well as of several closely related types of π-radicals, such as tyrosyl radicals or nitroxide spin labels [27, 28, 29, 30, 31]) was found to depend significantly on the presence or absence of hydrogen bonding [14, 15, 16, 17, 18, 19, 21, 32, 33]. Strong hydrogen bonding to the carbonyl oxygen atoms of the radical anions reduces the *g*-tensor anisotropy significantly (qualitative explanations are usually based on Stone's model [34, 35]). For example, the difference in the largest component of the *g*-tensor (g_x) of semiquinones measured in type I or type II photosynthetic reaction centers was taken as experimental evidence of the different strengths of hydrogen bonding in the corresponding active sites [36, 37, 38].

Early quantum chemical studies of semiquinone *g*-tensors used semiempirical methods and have provided important qualitative insights [39, 40, 41, 42, 43]. More recently, the use of accurate methods based on density functional theory (DFT) [44, 45] has allowed more quantitative calculations. In a systematic DFT study, we have used various cluster models, including explicit water or 2-propanol molecules, to study the effect of hydrogen bonding on semiquinone *g*-tensors in protic solution [46]. An extension of the study has provided new insights into protein environmental effects on semiquinone *g*-tensors, and thereby indirectly into the mechanism of photosystem I [47]. Multi-configuration

Contribution to the Jacopo Tomasi Honorary Issue

Correspondence to: M. Kaupp or I. Ciofini
e-mail: kaupp@mail.uni-wuerzburg.de
e-mail: ciofini@ext.jussieu.fr

self-consistent-field calculations on benzosemiquinone [48] and a recent two-component DFT study on a number of semiquinone-water clusters [49] should also be mentioned.

Generally, environmental effects may influence the *g*-tensor in two different ways: (a) *indirectly*, by modifying the structure of the radical (e.g. bond lengths or conformations), and (b) *directly*, by polarizing the electron density distribution and altering the ground-state wavefunction at a given geometrical structure. In the case of specific solvent-solute interactions, such as hydrogen bonding, cluster models as used previously may provide the most appropriate description. Nevertheless, the question of to what extent more long-range dielectric effects contribute in these cases remains. Moreover, unspecific solvent-solute interactions, e.g. in aprotic environments, might be described more efficiently by dielectric continuum models.

Although they have been widely used in NMR nuclear shielding calculations [50, 51, 52], to our knowledge dielectric continuum models have not yet been employed in the context of electronic *g*-tensors. In this work, we investigate the performance of Tomasi's polarizable continuum solvent model (PCM) [53, 54, 55] within the framework of uncoupled DFT (UDFT) [56, 57] calculations of *g*-tensors [44] for semiquinone radical anions in various solvents. In the case of protic solvents, the PCM model will be compared to—and combined with—model water cluster calculations.

The paper is organized as follows: after brief descriptions of the underlying theory for *g*-tensor calculations, and of the computational details, we discuss first the solvent effects on structures, as well as on charge and spin density distributions. Subsequently, solvent effects on *g*-tensors are discussed and analyzed, initially for benzosemiquinone and subsequently for a larger set of semiquinones.

Theory

A more general discussion on **g**-tensor calculations within the framework of DFT, and detailed descriptions of the method used here, may be found in [44, 58] and references therein. Here we summarize only the salient features needed to understand the results. The **g**-shift tensor, $\Delta\mathbf{g}$ (given in parts per million, ie in units of 10^{-6}), is computed as deviation from the free electron value, $g_e = 2002319...$:

$$\mathbf{g} = g_e\mathbf{1} + \Delta\mathbf{g} \tag{1}$$

Using second-order perturbation theory and taking into account the Breit-Pauli Hamiltonian terms up to $O(\alpha^2)$ [59], where α is the fine structure constant, the **g**-shift ($\Delta\mathbf{g}$) consists of three contributions:

$$\Delta\mathbf{g} = \Delta\mathbf{g}_{SO/OZ} + \Delta\mathbf{g}_{GC} + \Delta\mathbf{g}_{RMC} \tag{2}$$

The second-order spin-orbit/orbital Zeeman cross term, $\Delta g_{SO/OZ}$, generally dominates (except in the case of extremely small *g*-shifts). Local or gradient-corrected density functionals without exact-exchange admixture or explicit current dependence result in an UDFT approach [44, 56, 57], ie $\Delta\mathbf{g}_{SO/OZ}$ is computed as

$$\Delta g_{SO/OZ;u,v} = \frac{\alpha^2}{2} g_e \left[\sum_k^{occ(\alpha)} \sum_a^{virt(\alpha)} \frac{\langle \psi_k^\alpha | H_{SO,v} | \psi_a^\alpha \rangle \langle \psi_a^\alpha | \ell_{O,u} | \psi_k^\alpha \rangle}{\varepsilon_k^\alpha - \varepsilon_a^\alpha} - \sum_k^{occ(\beta)} \sum_a^{virt(\beta)} \frac{\langle \psi_k^\beta | H_{SO,v} | \psi_a^\beta \rangle \langle \psi_a^\beta | \ell_{O,u} | \psi_k^\beta \rangle}{\varepsilon_k^\beta - \varepsilon_a^\beta} \right] \tag{3}$$

where u and v are the cartesian components, H_{SO} are spatial parts of the one- and two-electron field-independent spin-orbit (SO) operators, ℓ_O is the spatial component of the orbital Zeeman operator, and ψ_i and ε_i are the Kohn-Sham spin orbitals and orbital energies, respectively.

Here, as in our previous studies of semiquinones [46, 47], SO matrix elements ($< H_{so} >$) are computed using the atomic mean field approximation (AMFI) [60, 61]. This approach has been shown to give results of comparable accuracy to an explicit Breit-Pauli treatment of the one- and two-electron SO matrix elements, at a fraction of the computational cost (this holds for *g*-tensors [44], as well as in calculations of SO corrections to NMR chemical shifts [62, 63]). Notably, this approach also accounts [44, 45] for the important spin-other-orbit terms (arising from the Breit interaction), which are neglected in other approximate DFT treatments. Furthermore, as the AMFI SO operators are one-center operators, a decomposition of the SO/OZ *g*-shift contribution into atomic contributions is still possible.

The kinetic energy correction to the spin-Zeeman interaction [up to $O(B_0)$], Δg_{RMC}, and the one-electron gauge correction, $\Delta g_{GC(1e)}$ are computed as [59]:

$$\begin{aligned} \Delta g_{RMC,uv} &= \tfrac{1}{2}\alpha^2 g_e \delta_{uv} \sum_{\lambda,\mu} P_{\lambda\mu}^{\alpha-\beta} \langle \chi_\mu | p^2 | \chi_\lambda \rangle \\ P_{\lambda\mu}^{\alpha-\beta} &= \sum_k^{occ(\alpha)} c_k^\lambda c_k^{\mu *} - \sum_k^{occ(\beta)} c_k^\lambda c_k^{\mu *} \\ \Delta g_{GC(1e),uv} &= \tfrac{1}{4}\alpha^2 g_e \sum_{\lambda,\mu} P_{\lambda\mu}^{\alpha-\beta} \left\langle \chi_\mu \left| \sum_M Z_M \frac{\delta_{\lambda\mu}(r_M \cdot r_O) - r_{M,u} r_{O,v}}{r_M^3} \right| \chi_\lambda \right\rangle \end{aligned} \tag{4}$$

where Z_M is the charge and R_M is the position of nucleus M, $p = -i\nabla$, P is the spin density matrix in the atomic orbital basis $\{\chi_\lambda\}$, and c_i^λ are the molecular orbital (MO) coefficients. The two-electron gauge correction term is currently neglected in our treatment. A common gauge at the center of nuclear charges was used for the external magnetic field.

Computational details

All structures were optimized at DFT level, using the gradient-corrected Becke exchange [64] and Perdew [65] correlation functionals (BP86). These calculations were carried out with the Gaussian98 program [66] and employed effective-core potentials (ECPs) with DZP valence basis sets for carbon and oxygen [67, 68], and a DZVP basis for hydrogen [69].

g-Tensors were also computed at the BP86 level (see [45, 46, 70, 71, 72] for comparative studies of *g*-tensors with different functionals), using an all-electron DZVP basis for all atoms [69]. This level of theory has been shown previously to provide accurate results for *g*-tensors of aromatic radicals [44, 46, 72]. Larger basis sets provide only small changes in the *g*-tensor components of semiquinones [46]. The underlying Kohn-Sham calculations were again done with the Gaussian98 program [66]. The computed MOs were used as input for the in-house property code MAG-ReSpect [73] (a recently implemented interface program [45] formatted the orbital information appropriately), with which the

g-tensor UDFT calculations were carried out, as described in the preceding section.

As in reference [45], but contrary to our previous calculations on semiquinones [46] which used the older version of the deMon program [74, 75], no fitting of exchange-correlation potential and charge density is used (i.e., four-center two-electron integrals are calculated explicitly). The discrepancies in the results (on the order of maximally 6% in Δg_x and Δg_y) between our present and previous calculations are due to these differences. At the same level of theory, dielectric solvent effects were treated within the polarizable continuum model (PCM) of Tomasi and co-workers [53, 54, 55]. More specifically, we used the conductor-like PCM model of Klamt [76], as implemented in Gaussian98 (CPCM) [77]. Calculations in water, dimethylsulfoxide (DMSO), tetrahydrofuran (THF), and acetonitrile were performed using standard UAHF radii [78] for the construction of the cavity. In order to separate *indirect* and *direct* solvent effects on *g*-tensors (see Introduction), two sets of calculations were performed: (a) single point calculations in a solvent at the gas-phase optimized structures (to determine only the *direct* solvent effect on the computed wavefunction), and (b) single point calculations at the solvent-optimized structures (the results incorporate both direct and indirect effects). Unless otherwise stated, the solvent results given pertain to (b), i.e., to the inclusion of both effects.

Since our calculations involved a generalized gradient approximation functional (BP86) and thus an UDFT approach (see above), as well as a common gauge origin, no coupling terms due to Hartree-Fock exchange or due to the continuum have been computed during the perturbation treatment. In other words, the *g*-shifts in solvent were computed as described in Eq. 3 and Eq. 4, but with the Kohn-Sham wavefunction obtained in self-consistent reaction field (SCRF) calculations for a given solvent. As in previous work, the following notation is used for the *g*-tensor components: g_x is oriented along the CO bond vector, g_y is perpendicular to the CO vector but still in the molecular plane, and g_z is perpendicular to the semiquinone plane.

Results and discussion

A schematic representation of the systems studied is shown in Fig. 1. Substituent effects on the *g*-tensors of semiquinones have been analyzed in detail previously (e.g., in [46] and references therein). Here we will focus on the solvent effects but note in passing that qualitatively the *g*-tensor anisotropy behaves like $BQ^{-\cdot} > DMBQ^{-\cdot} > DMEQ^{-\cdot} > DQ^{-\cdot} > NQ^{-\cdot} > DMNQ^{-\cdot}$ (see Fig. 1 for full names). This is due to increasing delocalization of spin density away from the carbonyl oxygen atoms, via conjugation to fused aromatic rings and/or via hyperconjugation to alkyl substituents. Ubisemiquinones have a relatively large *g*-anisotropy, due to a variety of reasons [46].

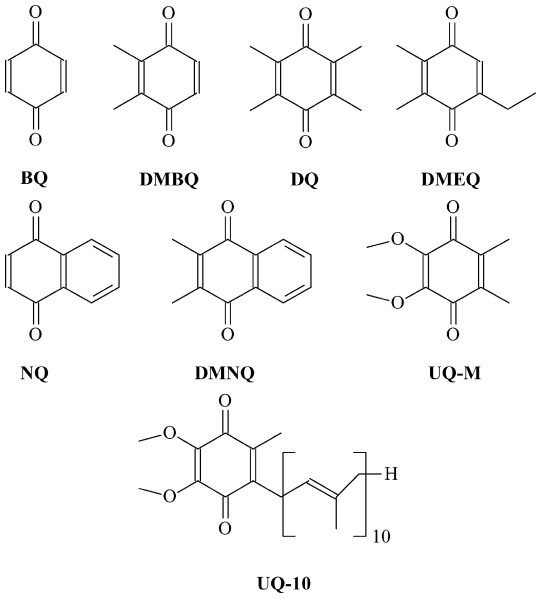

Fig. 1. 1,4-Quinone systems studied. *BQ* 1,4-benzoquinone, *DMBQ* 2,3-dimethyl-1,4-benzoquinone, *DMEQ* 2,3-dimethyl-5-ethyl-1,4-benzoquinone, *DQ* 2,3,4,6-tetramethyl-1,4-benzoquinone, *NQ* 1,4-naphthoquinone, *DMNQ* 2,3-dimethyl-1,4-naphthoquinone, *UQ-M* 2,3-dimethoxy-1,4-benzoquinone, *UQ-10* 2,3-dimethoxy–5-methyl-6-decaprenyl-4-benzoquinone

Solvent effects on structure, charge and spin density distribution

Relations between gas-phase optimized structural parameters, spin density distribution and *g*-tensors of semiquinones have already been discussed in detail [46]. For example, it is known that the *g*-shifts of semiquinones (in particular the SO/OZ contribution) are usually dominated by contributions of the oxygen and to a lesser extent of the *ipso* carbon atoms (see also below [46]). The SO/OZ contributions are related to the spin density on these atoms. Since this spin density depends mainly on the CO bond length, we will monitor the change of this distance from gas phase to solvent. From previous calculations, either in the presence of a solvent reaction field and/or of explicit solvent molecules [79], it is known that solvation favors polarization and charge separation (e.g. zwitterionic forms of the solute). In the present case, resonance structures with negative formal charge on oxygen and the unpaired electron on C_{ipso} of the phenyl ring, can be stabilized. This corresponds to increased charge separation in the CO bond. This qualitative expectation is indeed confirmed by the calculations. In Table 1, the CO distance, charge separation (difference in Mulliken charge) and the sum of spin densities (for $BQ^{-\cdot}$ only) for the C_{ipso} and O atoms are reported for the semiquinone in the gas phase and in the solvent reaction field (CPCM).

In case of the CPCM results, the localisation of charge on the O atoms with a consequent increase of the CO distance, is favoured with increasing solvent polarity, consistent with a reduced C-O bond order. This

Table 1. CO distance (in Å), Mulliken charge separation (Δq = C-O) and atomic Mulliken spin densities (n) for semiquinones in gas phase and in solution on an all electron DZVP basis

		Gas phase $\varepsilon = 1$	THF $\varepsilon = 7.58$	ACETO $\varepsilon = 36.64$	DMSO $\varepsilon = 46.7$	H_2O $\varepsilon = 78.39$
$BQ^{-\cdot}$	d(CO)	1.2670	1.2686	1.2690	1.2694	1.2727
	$\Delta q(C_{ipso}\text{-}O)$	0.707	0.728	0.731	0.733	0.762
	$n(C_{ipso})$	0.083	0.096	0.098	0.098	0.107
	n(O)	0.245	0.240	0.239	0.239	0.234
$DMBQ^{-\cdot}$	d(CO)	1.2696	1.2713	1.2717	1.2718	1.2745
	$\Delta q(C_{ipso}\text{-}O)$	0.672	0.682	0.682	0.683	0.708
$DMEQ^{-\cdot}$	d(CO)	1.2694	1.2718	1.2721	1.2721	1.2765
	$\Delta q(C_{ipso}\text{-}O)$	0.631	0.641	0.641	0.642	0.642
$DQ^{-\cdot}$	d(CO)	1.2723	1.2738	1.2743	1.2741	1.2766
	$\Delta q(C_{ipso}\text{-}O)$	0.603	0.619	0.619	0.620	0.640
$NQ^{-\cdot}$	d(CO)	1.2635	1.2654	1.2659	1.2659	1.2691
	$\Delta q(C_{ipso}\text{-}O)$	0.648	0.662	0.664	0.664	0.689
$DMNQ^{-\cdot}$	d(CO)	1.2662	1.2658	1.2680	1.2675	1.2711
	$\Delta q(C_{ipso}\text{-}O)$	0.605	0.609	0.605	0.605	0.632
$UQ^{-\cdot}$	d(CO)	1.2726	1.2732	1.2734	1.2733	1.2750
	$\Delta q(C_{ipso}\text{-}O)$	0.576	0.656	0.653	0.653	0.669

effect is largest for the smaller semiquinones, while it becomes almost negligible in the presence of a fused aromatic ring ($NQ^{-\cdot}$ and $DMNQ^{-}$).

A plot of CO distance *vs* charge separation for $BQ^{-\cdot}$ (Fig. 2) shows a virtually linear relationship ($R = 0.992$). Nevertheless, even with $\varepsilon_{H_2O} = 78.39$ the CO distance is still underestimated relative to results with explicit hydrogen bonds to water molecules. Obviously, stabilization of negative charge on the carbonyl oxygen atoms by direct hydrogen bonds is not simulated fully by a polarizable continuum. On the other hand, the effect of PCM on the cluster models is practically negligible, even for $[BQ(H_2O)_4]^{-\cdot}$. In the latter case, the four explicit water molecules describe well the first solvation sphere of $BQ^{-\cdot}$. Additionally, the cluster becomes less polarizable by the continuum (and polarizes the latter to a smaller extent) than isolated $BQ^{-\cdot}$. At the same time, the spin density decreases on oxygen and increases on the *ipso* carbon. While these variations in spin density are small, they are not negligible in the context of solvent

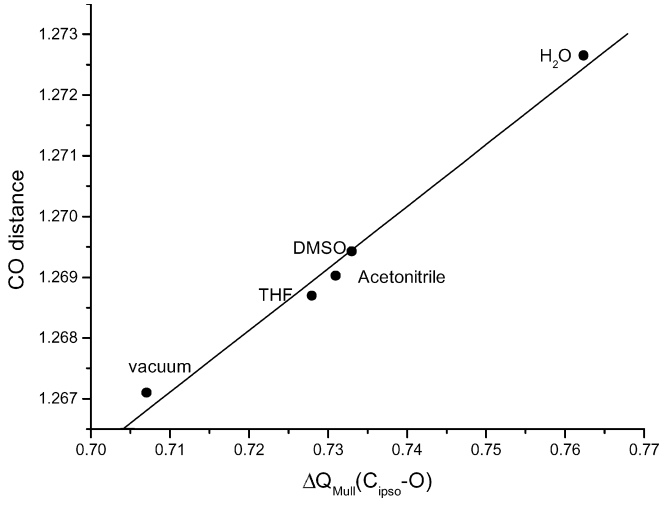

Fig. 2. Computed CO distance (in Å) vs. C-O charge separation for $BQ^{-\cdot}$ in the different environments vaccum, water, acetonitrile, dimethylsulfoxide (DMSO) and tetrahydrofuran (THF)

effects on g-shifts (see below). Again, the effect of explicit hydrogen bonds in cluster models is larger than that of a continuum model. On the other hand, spin delocalization onto the coordinated water molecules in the cluster is almost negligible (slight delocalization is found for strongly out-of-plane hydrogen bonds [46]). The hydrogen bonds affect mainly the in-plane highest doubly-occupied MO (HOMO), but have a much smaller effect on the out-of-plane singly-occupied MO (SOMO) (see below).

Interestingly, for the CPCM continuum model neither the spin density nor the charge separation change linearly with the solvent dielectric constant. For solvents with low dielectric constant (such as THF) small variations are found relative to the vacuum values. In contrast, large variations are seen for solvents with high dielectric constants (e.g. DMSO, acetonitrile, water). Overall, PCM reproduces qualitatively the expected solvent effects. However, the effects of explicit hydrogen bonds are underestimated significantly. To model the effect of protic solvents, the explicit inclusion of the first solvation sphere is obviously mandatory in order to obtain good molecular and electronic structures.

Analysis of solvent effects on g-tensor contributions for BQ-·

It is well known that, in particular, the largest g-tensor component in semiquinones, g_x, is very sensitive to interactions with the environment [36, 37, 38]. The main contributions arise from the $\Delta g_{SO/OZ}$ term (Eq. 4) [39, 40, 41, 42, 43, 46, 59, 80, 81], as shown by the data for $BQ^{-\cdot}$ in Table 2. Further insight thus requires the analysis of this second-order term. In our previous analyses of semiquinone g-tensors, we have mainly focused on an atomic break down of the SO/OZ cross term [46]. Here, we will instead use a recently implemented analysis [71] in terms of single excitations. Looking at Eq. 3, we may classify the excitations into three groups: (a) from doubly occupied orbitals to SOMO (D $\rightarrow$ S), (b) from

Table 2. Breakdown of gas-phase g-shift for $BQ^{-\cdot}$[a]. D Doubly occupied MOs, V virtual MOs

		Δg_x	Δg_y	Δg_z
Δg_{tot}		6530	3065	−20
$\Delta g_{GC(1e)}$		200	316	229
Δg_{RMC}		−237	−237	−237
$\Delta g_{SO/OZ}$		6567	2987	−13
$\Delta g_{SO/OZ}$	Σ(SOMO → V)	−423	−29	0
	Σ(D → SOMO)	7012	3018	0
	(HOMO → SOMO)	5916	0	0
	Σ(D → V)	−37	8	−44

[a]Cf. Eq. 3 and Eq. 4

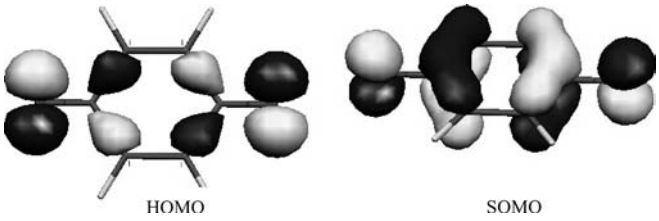

Fig. 3. Isodensity surface (±0.025 au) for frontier orbitals of $BQ^{-\cdot}$ in the gas phase. *HOMO*: in-plane highest doubly-occupied molecular orbital, *SOMO*: out-of-plane singly-occupied molecular orbital

SOMO to virtual orbitals (S → V), and (c) from doubly occupied to virtual orbitals (D → V) (the latter arise from spin polarization and are hence usually small). The SO/OZ contributions due to each of these three groups of excitations are presented in Table 2. Obviously, g_x of $BQ^{-\cdot}$ in vacuum is dominated by the D → S contributions, and in particular by the HOMO → SOMO excitation. This agrees with qualitative models [32], and with previous computational results for semiquinones and phenoxyls [27, 28, 29, 30, 39, 40, 41, 42, 43, 48]. Figure 3 shows that the SOMO is the well-known out-of-plane π MO, with large coefficients at oxygen and C_{ipso}, whereas the HOMO corresponds largely to an in-plane MO (O-C_{ipso} antibonding, C_{ipso}-C_{ortho} bonding) with large contributions on oxygen. In order to significantly reduce g_x, the solvent has to either increase the HOMO-SOMO energy gap (denominator in Eq. 3) or decrease the orbital Zeeman term (OZ) and/or SO matrix elements (numerator in Eq. 3). A corresponding analysis for g_x of $BQ^{-\cdot}$ in different environments, focusing on the dominant contribution of the HOMO-SOMO excitation, is shown in Table 3. First of all, we note that both SO and OZ matrix elements are reduced by solvation. This reflects a reduced oxygen spin density (and an enhancement on C_{ipso} [37]). Simultaneously, the HOMO-SOMO gap increases, in particular due to a stabilization of the HOMO. While the CPCM results suggest that changes in the energy denominator are about three times more important than changes in the matrix elements, our cluster calculations suggest that all of these changes contribute to a very similar extent to the overall reduction of Δg_x when hydrogen bonding is involved. In particular, the reduction of the SO matrix elements using cluster models with respect to CPCM is related to an increase of computed spin polarisation when going from CPCM calculations to cluster approaches. This is related to the neglect of both direct spin polarisation and Pauli repulsion in the CPCM model. A quantitative evaluation of their relative role is not possible. Nevertheless, since the direct interaction with the solvating water molecules affects mainly the HOMO, a small direct spin delocalisation to the solvent molecules is found in the cluster models.

The values reported in Table 3 refer to calculations in solvent at the solvent-optimized structures, i.e., both indirect and direct effects are included. Calculations using the vacuum structures and thus only including the direct effects provide a less pronounced stabilization of the HOMO, but a larger *destabilization* of the SOMO, compared to calculations at the gas-phase optimised structure without inclusion of the solvent reaction field. This is mainly due to the fact that the elongation of the CO bond in solution allows a stabilization of the CO antibonding HOMO and SOMO orbitals, which is not accounted for when employing the gas phase structure. Neglecting the structural relaxation in solution leads thus to g_x values which are too small compared to the fully relaxed calculations (cf. Table 4 below).

A plot of Δg_x versus $\Delta\varepsilon_{(HOMO\text{-}SOMO)}$ computed for $BQ^{-\cdot}$ in different solvents (Fig. 4) shows an essentially linear dependence ($R = 0.999$). This confirms that the transition from HOMO to SOMO dominates g_x. Explicit inclusion of water molecules allows a better stabilization of HOMO versus SOMO since these molecules interact directly with the in-plane oxygen lone pairs. As a consequence, the HOMO-SOMO gap computed in cluster models is larger and the reduction in g_x is more pronounced than in the CPCM calculations (similarly, the reduction of the SO and OZ matrix elements is more pronounced in the cluster models, see above).

Substituted semiquinones: comparison with experiment

Unfortunately, a direct comparison with experiment in aprotic solvents is difficult since very few experiments in

Table 3. Breakdown of the HOMO-SOMO contribution to $\Delta g_{x,SO/OZ}$ for $BQ^{-\cdot}$ in different environments. HOMO and SOMO β orbital energies in au, $<OZ>_{H\to S}$ in 10^{-4} eV/T, $<SO>_{H\to S}$ in 10^{-4} eV, and g_x contribution in ppm

	$BQ^{-\cdot}$	$BQ^{-\cdot}{}_{THF}$	$BQ^{-\cdot}{}_{DMSO}$	$BQ^{-\cdot}{}_{ACETO}$	$BQ^{-\cdot}{}_{H2O}$	$[BQ(H_2O)_4]^{-\cdot}$
ε_{HOMO}	−0.027	−0.157	−0.174	−0.173	−0.192	−0.095
ε_{SOMO}	0.038	−0.090	−0.107	−0.106	−0.123	−0.024
$\Delta\varepsilon$	0.065	0.067	0.067	0.067	0.069	0.071
$<SO>_{H\to S}$	49.80	49.22	49.14	49.11	48.40	43.02
$<OZ>_{H\to S}$	0.617	0.612	0.611	0.611	0.602	0.495

Table 4. Computed *g*-shift components (in ppm) for semiquinone radical anions. Results are at solvent-optimized structure with results at gas-phase structure in parentheses

	Δg_{iso}	Δg_x	Δg_y	Δg_z
$BQ^{-\cdot}$	3190	6530	3065	−20
$BQ^{-\cdot}{}_{THF}$	3091(3043)	6285(6113)	3012(2980)	−23 (−23)
$BQ^{-\cdot}{}_{Acetonitrile}$	3076(3023)	6247(6113)	3004(2980)	−24 (−24)
$BQ^{-\cdot}{}_{DMSO}$	3083(3022)	6265(6110)	3007(2980)	−24 (−24)
$BQ^{-\cdot}{}_{H2O}$	2987(2889)	6024(5778)	2964 (2915)	−27 (−27)
$[BQ(H_2O)_4]^{-\cdot}$	2608	4889	2935	+2
$[BQ(H_2O)_4]^{-\cdot}{}_{H2O}$	2557	4787	2906	−23
exp[a]	2350	4130	2940	−30
$DMBQ^{-\cdot}$	3061	6131	3057	−3
$DMBQ^{-\cdot}{}_{THF}$	2997	5989	3008	−5
$DMBQ^{-\cdot}{}_{Acetonitrile}$	2987	5968	3000	−5
$DMBQ^{-\cdot}{}_{DMSO}$	2989	5973	3000	−5
$DMBQ^{-\cdot}{}_{H2O}$	2912	5784	2957	−8
$[DMBQ(H_2O)_4]^{-\cdot}$	2509	4716	2817	−30
$[DMBQ(H_2O)_4]^{-\cdot}{}_{H2O}$	2421	4545	2784	−67
exp[a]	2240	3870	2900	−60
$DMEQ^{-\cdot}$	2917	5751	3002	−2
$DMEQ^{-\cdot}{}_{THF}$	2856	5625	2947	−3
$DMEQ^{-\cdot}{}_{Acetonitrile}$	2843	5592	2938	−4
$DMEQ^{-\cdot}{}_{DMSO}$	2841	5590	2937	−4
$DMEQ^{-\cdot}{}_{H2O}$	2778	5445	2897	−7
$[DMEQ(H_2O)_4]^{-\cdot}$	2337	4397	2687	−74
$[DMEQ(H_2O)_4]^{-\cdot}{}_{H2O}$	2317	4319	2683	−45
exp[a]	2160	3820	2800	−130
$DQ^{-\cdot}$	2837	5510	3016	−13
$DQ^{-\cdot}{}_{THF}$	2795	5428	2973	−15
$DQ^{-\cdot}{}_{Acetonitrile}$	2792	5425	2968	−16
$DQ^{-\cdot}{}_{DMSO}$	2789	5416	2966	−16
$DQ^{-\cdot}{}_{H2O}$	2734	5295)	2926	−18
$[DQ(H_2O)_4]^{-\cdot}$	2320	4397	2646	−95
$[DQ(H_2O)_4]^{-\cdot}{}_{H2O}$	2273	4319	2632	−84
exp[a]	2160	3790	2800	−100
exp.in MTHF[b]	2380	4380	2910	−140
$NQ^{-\cdot}$	2850	5627	2898	25
$NQ^{-\cdot}{}_{THF}$	2795	5428	2973	24
$NQ^{-\cdot}{}_{Acetonitrile}$	2750	5388	2840	24
$NQ^{-\cdot}{}_{DMSO}$	2750	5387	2840	24
$NQ^{-\cdot}{}_{H2O}$	2656	5161	2786	22
$[NQ(H_2O)_4]^{-\cdot}$	2259	4145	2630	1
$[NQ(H_2O)_4]^{-\cdot}{}_{H2O}$	2177	3959	2578	−6
exp[a]	2060	3500	2730	−40
$DMNQ^{-\cdot}$	2588	4934	2829	2
$DMNQ^{-\cdot}{}_{THF}$	2385	4475	2684	−3
$DMNQ^{-\cdot}{}_{Acetonitrile}$	2412	4542	2698	−3
$DMNQ^{-\cdot}{}_{DMSO}$	2405	4526	2694	−4
$DMNQ^{-\cdot}{}_{H2O}$	2321	4326	2644	−7
$[DMNQ(H_2O)_4]^{-\cdot}$	2060	3811	2484	−116
exp[a]	1970	3360	2650	−100
$UQ^{-\cdot}$	2792	5194	3256	−74
$UQ^{-\cdot}{}_{THF}$	2779	5162	3248	−74
$UQ^{-\cdot}{}_{Acetonitrile}$	2781	5169	3247	−73
$UQ^{-\cdot}{}_{DMSO}$	2778	5162	3248	−74
$UQ^{-\cdot}{}_{H2O}$	2722	5030	3207	−71
$[UQ(H_2O)_4]^{-\cdot}$	2496	4538	2955	−4
$[UQ(H_2O)_4]^{-\cdot}{}_{H2O}$	2475	4383	3001	41
exp(UQ-10)[a]	2210	3900	2940	−220

[a][14,15,16,17]
[b][80,81]

pure aprotic solution have been performed as yet. Currently, the only available data are the *g*-tensor of $DQ^{-\cdot}$ in 2-methyltetrahydrofuran (MTHF), and the one of UQ-$3^{-\cdot}$ measured in a dimethoxyethane (DME)/MTHF mixture [82]. The computed $\Delta g_x = 5428$ ppm for $DQ^{-\cdot}$ in THF (Table 4) is considerably larger than the measured $\Delta g_x = 4380$ ppm in MTHF. On the other hand, the computed $\Delta g_{iso} = 3083$ ppm for $BQ^{-\cdot}$ in DMSO (Table 4) agrees reasonably well with the corresponding experimental DMSO-value, $\Delta g_{iso} = 3200$ ppm [33].

In view of this lack of suitable experimental data in aprotic solvents, we will in the following concentrate on values measured in protic frozen 2-propanol solution.

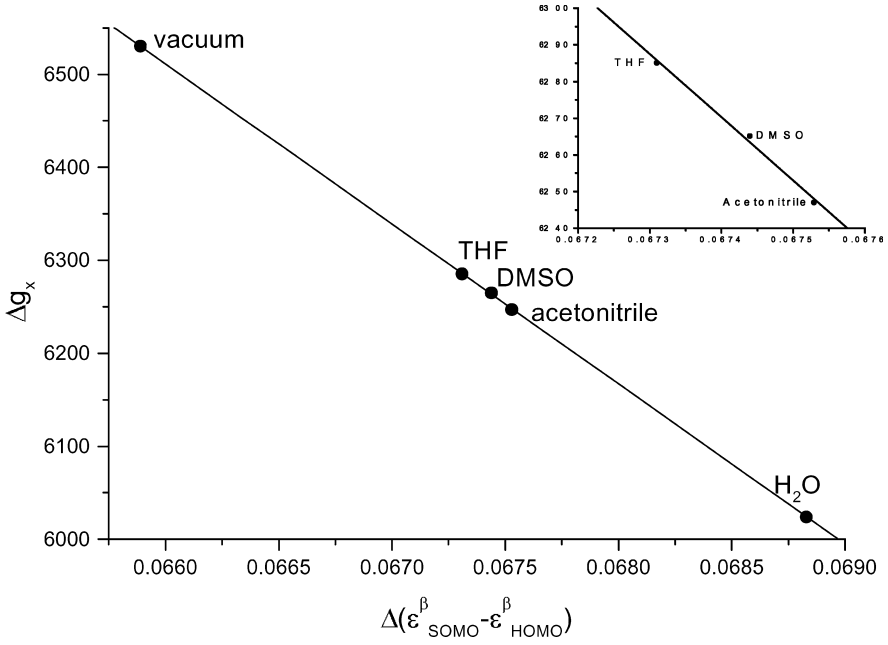

Fig. 4. Computed Δg_x values (in ppm) for $BQ^{-\cdot}$ in different solvents vs. HOMO-SOMO energy gap (in au)

These data are available for all of the systems studied here except for UQ-$M^{-\cdot}$ where we will compare to results for UQ-$10^{-\cdot}$ (see Fig. 1). The computational results considered here are in H_2O solvent. For explicit supermolecular cluster calculations with 2-propanol molecules, the reader is referred to [46]. Due to the somewhat stronger hydrogen bonds with 2-propanol compared to water, the reduction of Δg_x in these models is slightly more pronounced than with water molecules [46]. Figure 5 compares computed g_x values for the free semiquinone, for the cluster models ($[Q(H_2O)_4]^{-\cdot}$) in vacuum, and for the cluster embedded in CPCM water solvent reaction field ($\varepsilon = 78.39$). As discussed previously [46], calculations on the unsolvated, free radical anions overestimate Δg_x by ca. 50%, except for UQ-$M^{-\cdot}$ where seemingly the computed Δg_x agrees "too well" with the experimental value for UQ-$10^{-\cdot}$ (see Table 4). As discussed in [46], the reason in the latter case is a structural one: while the preferred out-of-plane C-C-O-CH_3 dihedral angles for the methoxy groups in the free gas phase radical are ca. 56°, the groups are more strongly out-of-plane for solvated cluster models (C-C-O-CH_3 dihedral angle ca.110°). The overall effect of the larger C-OCH_3 dihedral upon g_x is a significant increase (ca. 600 ppm for both groups at 110° vs 56° [46]). This leads to a better linear correlation with the other semiquinones (i.e. the results for UQ-$M^{-\cdot}$ are now also in worse agreement with experiment). The results reported here refer always to fully relaxed UQ-$M^{-\cdot}$ or $[UQ\text{-}M(H_2O)_4]^{-\cdot}$structures. To avoid confusion or artefacts, the results for UQ-$M^{-\cdot}$ have therefore been omitted from the linear regression analyses.

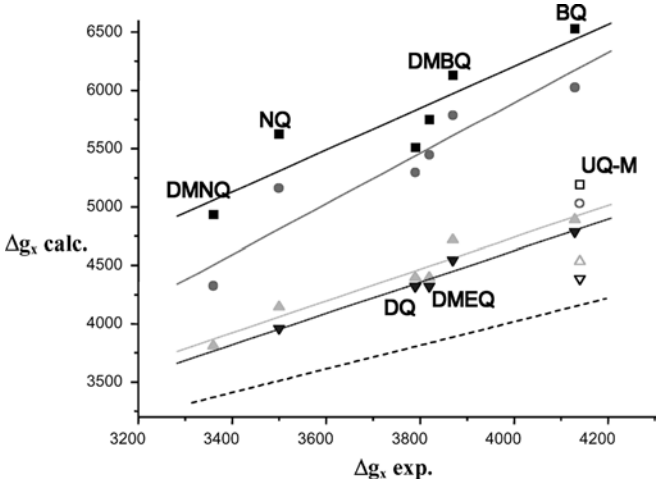

Fig. 5. Computed Δg_x values (in ppm) for semiquinones in vacuum (*squares*), in H_2O with conductor-like polarizable continuum model (*CPCM*) (*circles*), for $[Q(H_2O)_4]^{-\cdot}$ cluster models in vacuum (*up triangles*), and for $[Q(H_2O)_4]^{-\cdot}$ in H_2O with CPCM (*down triangles*), relative to experimental data in 2-propanol

There is a modest linear correlation ($R = 0.91$) between the computed gas-phase g_x values and experimental data in 2-propanol (Table 4, Table 5), but the slope is much too large (see also [46]). When including

Table 5. Results of linear regression analysis for Δg_x and Δg_y computed with and without solvent models in comparison with the experimental data. UQ-$M^{-\cdot}$ results were omitted from the regression analysis. $\Delta g_i = A + B \times \Delta g_i$, *SD* standard deviation in ppm, *R* correlation coefficient

	Δg_x				Δg_y			
	A	B	R	SD	A	B	R	SD
$Q^{-\cdot}$	−973	1.8	0.91	259	613	0.8	0.96	31
$Q^{-\cdot}{}_{H2O}$	−2145	1.9	0.93	235	−180	1.0	0.92	52
$[Q^{-\cdot}(H_2O)_4]$	−702	1.4	0.97	109	−1333	1.4	0.98	37
$[Q^{-\cdot}(H_2O)_4]_{H2O}$	−743	1.3	0.98	68	−1522	1.4	0.98	34

the environment via the CPCM model, the g_x values decrease. The reduction increases with increasing dielectric constant of the solvent. However, as discussed above, the reduction in g_x is not directly proportional to ε. The correlation between the g_x values computed in H_2O and the experimental one is improved ($R = 0.93$) with respect to the values computed in vacuum. However, the absolute effect on g_x is only ca. 200–300 ppm, roughly 10% of the effect obtained upon adding explicitly four water molecules (in the latter case, $R = 0.96$ also indicates a better description), and thus the slope is still much too large (Table 5). The best performance is found when adding the PCM model to the supermolecular cluster. This reduces Δg_x by another few hundred parts per million and brings it closer to experiment ($R = 0.98$), with a correspondingly reduced slope. As discussed previously [46], supermolecular results with 2-propanol provide a still smaller slope and after scaling by a factor 0.92 agree with experiment essentially within experimental accuracy. However, already the $[Q(H_2O)_4]_{H2O}$ results (Table 4, Table 5) are very suitable to discuss substituent effects on Δg_x.

While Δg_z is too small to be discussed meaningfully, we should also examine Δg_y. Table 2 shows that the main SO/OZ contribution to Δg_y arises from $D \rightarrow S$ excitations, in particular from an energetically low-lying σ(C-O)-bonding doubly occupied MO. The latter is less sensitive to polarization by the environment than the π-type HOMO. In consequence, solvent effects on Δg_y are considerably less pronounced than those on Δg_x, while following the same trends.

Conclusions

Previous supermolecular cluster DFT calculations of solvent effects on the *g*-tensors of semiquinone radical anions have been extended to incorporate a polarizable dielectric continuum model (Tomasi's PCM). To our knowledge this has been the first application of continuum models to electronic *g*-tensors.

The dielectric continuum reduces in particular the Δg_x component of semiquinones, and to a lesser extent also Δg_y. This arises to a large extent from the lengthening of the carbonyl C-O bond, but the direct polarization of the wavefunction at a given structure is also important, via an enhanced HOMO-SOMO gap and via reduced SO and OZ matrix elements. In the case of protic solvents, the CPCM model alone recovers only a fraction of the specific solvent interactions. In this case inclusion of the first solvent shell by a cluster model is mandatory. Then the dielectric continuum helps to further improve the agreement between computed and experimental Δg_x. This is consistent with previous findings for other magnetic properties of molecules in solution within the PCM framework [83, 84]. Comparison with experiment for aprotic solvents is currently difficult, due to the relative scarcity of experimental data. The present results should be helpful as an orientation for further high-field EPR work in different solvents.

Acknowledgements. We thank Carlo Adamo (Paris), Olga L. Malkina, and Vladimir G. Malkin (Bratislava) for helpful suggestions. This study has been supported by the graduate college Moderne Methoden der magnetischen Resonanz in der Materialforschung at Universität Stuttgart (scholarship to I.C.), Deutsche Forschungsgemeinschaft (Priority Program SP1051, "High-Field EPR", project Ka1187/4), and by Fonds der Chemischen Industrie.

References

1. Yang F, Shen G, Schlucther WM, Zybailov B, Ganago AO, Vassiliev IR, Bryant DA, Goldbeck JH (1998) J Phys Chem B 102:8288
2. Kamlowski A, Zech SG, Fromme P, Bittl R, Lubitz W, Witt HT, Stehlik DJ (1998) Phys Chem B 102:8266
3. Rohrer M, MacMillan F, Prisner TF, Gardiner AT, Möbius K, Lubitz WJ (1998) Chem Phys B 102:4648
4. Calvo R, Abresch EC, Bittl R, Feher G, Hofbauer W, Isaacson RA, Lubitz W, Okamura MY, Paddock ML (2000) J Am Chem Soc 122:7327
5. Calvo R, Isaacson RA, Paddock ML, Abresch EC, Okamura MY, Maniero AL, Brunel L-C, Feher G (2001) J Chem Phys B 105:4053
6. Rigby EEJ, Evans MCW, Heathcote P (1996) Biochemistry 35:6651
7. Prisner TF, van der Est A, Bittl R, Lubitz W, Stehlik D, Möbius K (1995) Chem Phys 194:361
8. Deligiannakis Y, Boussac A, Rutherford AW (1995) Biochemistry 34:16030
9. Ostafin AE, Weber S (1997) Biochim Biophys Acta 195:1320
10. Hanley J, Deligiannakis Y, MacMillan F, Bottin H, Rutherford AW (1997) Biochemistry 36:11543
11. Link G, Berthold M, Weidner J-U, Ohmes E, Tang J, Poluekto'v O, Utschig L, Schlesselman SL, Thurnauer MC, Kothe G (2001) J Am Chem Soc 123:4211
12. Bittl R, Zech SG, Fromme P, Witt HT, Lubitz W (1997) Biochemistry 36:12001
13. Bittl R, Zech SG (1997) J Phys Chem B 101:1429
14. Burghaus O, Plato M, Rohrer M, Möbius K, Macmillan F, Lubitz W (1993) J Phys Chem 97:7639
15. Rohrer M, Plato M, Macmillan F, Grishin Y, Lubitz W, Möbius K (1995) J Mag Reson 116:59
16. MacMillan F, Lendzian F, Lubitz W (1995) Magn Reson Chem 33:81
17. MacMillan F, Hanley J, van der Weerd L, Knüpling M, Un S, Rutherford AW (1997) Biochemistry 36:9297
18. Lubitz W, Feher G (1999) Appl Magn Reson 17:1
19. Levanon H, Möbius K (1997) Annu Rev Biophys Biomol Struct 26:495
20. Patai S (1974) Chemistry of quinoid compounds. Interscience, New York
21. Pedersen JA (1985) EPR spectra from natural and synthetic quinones and quinoids. CRC, Boca Raton, Fla.
22. O'Malley PJ, Babcock GT (1984) J Chem Phys 80:3912
23. O'Malley PJ, Babcock GT (1986) J Am Chem Soc 108:3995
24. Lubitz W, Abresch EC, Debus RJ, Isaacson RA, Okamura MY, Feher G (1985) Biochim Biophys Acta 808:464
25. Van der Brink JS, Hulsebosch RJ, Gastl P, Hore PJ, Hoff AJ (1994) Biochemistry 33:13668
26. Kamlowski A, Altenberg-Greulich B, van der Est A, Zech SG, Bittl R, Fromme P, Lubitz W, Stehlik D (1998) J Phys Chem B 192:8278
27. Un S, Atta M, Fontcave M, Rutherford AW (1995) J Am Chem Soc 117:10713
28. Ivancich A, Mattioli TA, Un S (1999) J Am Chem Soc 121:5743
29. Un S, Gerez C, Elleingard E, Fontecave M (2001) J Am Chem Soc 123:3048

30. Liu A, Barra A-L, Rubin H, Lu G, Gräslund A (2000) J Am Chem Soc 122:1974
31. Owenius R, Engström M, Lindgren M, Huber M (2001) J Phys Chem A 105:10967
32. Hales BJ (1975) J Am Chem Soc 97:5993
33. Zandstra PJ (1964) J Chem Phys 41:3655
34. Stone A (1963) J Proc R Soc A 271:424
35. Stone A (1964) J Mol Phys 6:316
36. van der Est A, Sieckmann I, Lubitz W, Stehlik D (1995) Chem Phys 194:349
37. Zech SG, Hofbauer W, Kamlowski A, Fromme P, Stehlik D, Lubitz W, Bittl R (2000) J Phys Chem B 104:9728
38. van der Est A, Prisner TF, Bittl R, Fromme P, Lubitz W, Möbius K, Stehlik D (1997) J Phys Chem B 101:1437
39. Angstl R (1989) Chem Phys 132:435
40. Plakhutin BN, Zhidomirov GM, Zamaraev, KI (1983) J Struct Chem 24:3
41. Un S, Atta M, Fontcave M, Rutherford AW (1995) J Am Chem Soc 117:10713
42. Knüpling M, Törring JT, Un S (1996) Chem Phys 219:291
43. Törring JT, Un S, Knüpling M, Plato M, Möbius K (1997) J Chem Phys 107:3095
44. Malkina O, Vaara J, Schimmelpfennig B, Munzarová M, Malkin VG, Kaupp M (2000) J Am Chem Soc 122:9206
45. Kaupp M, Reviakine R, Malkina OL, Arbuznikov A, Schimmelpfennig B, Malkin VG (2002) J Comput Chem 23:794
46. Kaupp M, Remenyi C, Vaara J, Malkina OL, Malkin VG (2002) J Am Chem Soc 124:2709
47. Kaupp M (2002) Biochemistry 40:2895
48. Engström M, Vahtras O, Ågren H (1999) Chem Phys 243:263
49. Neyman KM, Ganyushin DI, Rinkevičius Ž, Rösch N (2002) Int J Quantum Chem 90:1404
50. Cammi R (1998) J Chem Phys 109:3185
51. Cammi R, Mennucci B, Tomasi J (1999) J Chem Phys 110:7627
52. Tomasi J, Cammi R, Mennucci B, Cappelli C, Corni S (2002) Phys Chem Chem Phys 4:5967
53. Miertus S, Scrocco E, Tomasi J (1981) Chem Phys 55:117
54. Cammi R, Tomasi J (1995) J Comp Chem 16:1449
55. Tomasi J, Persico M (1995) Chem Rev 94:2027
56. Malkin VG, Malkina OL, Casida ME, Salahub DR (1994) J Am Chem Soc 116:5898
57. Malkin VG, Malkina OL, Eriksson LA, Salahub DR (1995) The calculation of NMR and ESR spectroscopy parameters using density functional theory. In: Seminario JM, Politzer P (eds) Modern density functional theory: a tool for chemistry; theoretical and computational chemistry, vol 2. Elsevier, Amsterdam
58. Kaupp M (2003) Ab initio and density functional calculations of electronic *g*-tensors for organic radicals. In: Lund A, Shiotani M (eds) EPR spectroscopy of free radicals in solids trends in methods and applications. Kluwer, Dordrecht
59. Harriman JE (1978) Theoretical foundations of electron spin resonance. Academic, New York
60. Hess B, Marian CM, Wahlgren U, Gropen O (1996) Chem Phys Lett 251:365
61. Schimmelpfennig B (1996) Atomic spin-orbit mean-field integral program. Stockholms Universitet, Sweden
62. Malkina OL, Schimmelpfennig B, Kaupp M, Hess B, Chandra P, Wahlgren U, Malkin VG (1998) Chem Phys Lett 296:93
63. Vaara J, Malkina OL, Stoll H, Malkin VG, Kaupp M (2001) J Chem Phys 114:61
64. Becke AD (1988) Phys Rev A 38:3098
65. Perdew JP (1986) Phys Rev B 33:8822
66. Frisch MJ, Trucks GW, Schlegel HB, Scuseria GE, Robb MA, Cheeseman JR, Zakrzewski VG, Montgomery Jr JA, Stratmann RE, Burant JC, Dapprich S, Millam JM, Daniels AD, Kudin KN, Strain MC, Farkas O, Tomasi J, Barone V, Cossi M, Cammi R, Mennucci B, Pomelli C, Adamo C, Clifford S, Ochterski J, Petersson GA, Ayala PY, Cui Q, Morokuma K, Malick DK, Rabuck AD, Raghavachari K, Foresman JB, Cioslowski J, Ortiz JV, Baboul AG, Stefanov BB, Liu G, Liashenko A, Piskorz P, Komaromi I, Gomperts R, Martin RL, Fox DJ, Keith T, Al-Laham MA, Peng CY, Nanayakkara A, Gonzalez C, Challacombe M, Gill PMW, Johnson B, Chen W, Wong MW, Andres JL, Gonzalez C, Head-Gordon M, Replogle ES, Pople JA (1998) Gaussian 98, Revision A7. Gaussian, Pittsburgh, Pa.
67. Bergner A, Dolg M, Küchle W, Stoll H, Preuss H (1993) Mol Phys 80:1431
68. Huzinaga S (1984) Gaussian basis sets for molecular calculations. Elsevier, New York
69. Godbout N, Salahub DR, Andzelm J, Wimmer E (1992) Can J Chem 70:560
70. Neese F (2001) J Chem Phys 115:11080
71. Kaupp M, Asher J, Arbuznikov A, Patrakov A (2002) Phys Chem Chem Phys 4:5466
72. Kaupp M, Gress T, Reviakine R, Malkina OL, Malkin VJ (2003) Phys Chem B 107:331
73. Malkin VG, Malkina OL, Reviakine R, Schimmelpfennig B, Arbuznikov A, Kaupp M (2001) MA*G*-ReSpect, version 10
74. Salahub DR, Fournier R, Mlynarski P, Papai I, St-Amant A, Ushio J (1991) deMon program. In: Labanowski J, Anzelm J (eds) Density functional methods in chemistry. Springer, Berlin Heidelberg New York
75. St-Amant A, Salahub DR (1990) Chem Phys Lett 169:387
76. Klamt A, Schüürman G (1993) J Chem Soc Perkins Trans 2:799
77. Barone V, Cossi M (1998) J Phys Chem A 102:1995
78. Barone V, Cossi M, Tomasi, J (1997) J Chem Phys 107:3210
79. Adamo C, Subra R, Di Matteo A, Barone V (1998) J Chem Phys 109:10244
80. Lushington GH, Grein F (1996) Theor Chim Acta 93:259
81. Schreckenbach G, Ziegler T (1997) J Phys Chem A 101:3388
82. Nimz O, Lendzian F, Boullais C, Lubitz W (1998) Appl Magn Reson 14:255
83. Mennucci B (2002) J Am Chem Soc 124:1506
84. Adamo C, Cossi M, Rega N, Barone V (2001) Theoretical biochemistry–process and properties of biological systems, theoretical and computational chemistry. Elsevier Science